Fabrication and Characterization of Mg(OH)$_2$ Films on AZ31 Magnesium Alloy by Alkali Treatment

Hui Tang[1,2,3,4][*], *Tao Wu*[1], *Fangjun Xu*[3], *Wei Tao*[1], *Xian Jian*[1,*]

[1] School of Energy Science and Engineering, University of Electronic Science and Technology of China. Chengdu, 610000, China
[2] Center for Information in BioMedicine，University of Electronic Science and Technology of China, Chengdu, 610054, China
[3] Shanxi Key laboratory of advanced magnesium-based materials, Taiyuan University of Technology, Taiyuan 030024, PR China
[4] School of Chemical Engineering and Technology, Harbin Institute of Technology, Harbin 150001, China
[*]E-mail: tanghui@uestc.edu.cn, jianxian@uestc.edu.cn

Mg and its alloys have shown potential application as a bio-absorbable biomaterial, such as for bone screws and plates, however, their fast corrosion rate may result in the sudden failure of the implants. In this paper, compact and dense films are formed on AZ31 magnesium alloy by alkali treatment. The microstructure and composition of the films are examined by SEM, EDS and XRD, respectively. The bonding strength and corrosion behaviour of the films are characterized by tensile strength test, potentiodynamic polarization and electrochemical impedance spectroscopy (EIS) studies. The results show that the main composition of the films is Mg(OH)$_2$, the bonding strength between the film and the substrate is stronger than 60 MPa. And the corrosion resistance is improved by the alkali treatment compared with that of the bare AZ31 magnesium alloy in the simulated body fluid (SBF) solution. It is increased with increasing the treatment time.

1. INTRODUCTION

Magnesium and its alloys have attracted widely attention as a new biodegradable materials for implant applications. Magnesium has similar mechanical properties to natural bone. Notably, the elastic modulus of magnesium (~ 45 GPa) is close to that of natural bone (3~20 GPa) [1, 2]. This attractive property can reduce the risk of stress shielding effect in orthopedic applications, and

accelerate the healing process [3, 4]. Furthermore, magnesium is the fourth most abundant cation in human body, and is naturally found in bone tissue. Magnesium has significant functional roles in biological systems and bone tissue, which can stimulate effects on the growth of new bone tissue [5]. In addition, the second surgery for removal of the metal bone plates and screws is not necessary, owing to the biodegradability and bioabsorbability of magnesium in human body. However, the rapid corrosion of magnesium and its alloys in human body fluid has limited their clinical application. If magnesium alloys are designed to implants, they may lose the mechanical property before the healing of bone tissue due to the rapid corrosion [6, 7]. Therefore, it is extremely important to improve the corrosion resistance of magnesium alloys for their biomedical application.

Several coating techniques have been investigated to improve the corrosion resistance of magnesium alloys, including the electrochemical deposition, chemical conversion, biomimetic coatings anodizing, sol–gel method, ion-beam assisted deposition, and alkali-heat-treatment [10-14]. However, most of these treatments have a lot of drawbacks. For example, the adhesion can be an issue in the case of electrochemical deposition or chemical conversion. The alkali-heat-treatment and ion-beam assisted deposition may inferior the mechanical properties of the substrate. Alkali treatment is a relatively convenient and effective technique to deposit layers on the substrates of titanium, iron and their alloys [15, 16]. Moreover, it is a low-temperature process and suitable for the formation of uniform coatings on the substrates with complex geometries. Additionally, it is a simple and cost-effective way. Successful researches to prepare alkali treatment films on magnesium alloys have been reported [17-19]. Most of the experiment have been conducted in an autoclave, and a high temperature is required. In this case, modification for post traumatic plate is difficult because it need autoclave [20, 21]. For the application view, it needs to decrease the treatment temperature, and reduce the cost of the treatment. In this study, the preparation temperature is lower than 100 ^{o}C. And the processes is completed at atmospheric.

In the following section, we introduce an alkali treatment processes for magnesium-based alloys. The influences of treatment time on the structure, composition, adhesion strength of the films have been investigated. The corrosion behavior of the films is also studied by potentiodynamic polarization tests and electrochemical impedance spectroscopy in a simulated body fluids solution.

2. EXPERIMENTAL AND METHOD

2.1 Surface treatments

Rectangular coupons of AZ31 Mg alloy of dimensions 20 mm ×20 mm ×2 mm were used as the substrate material. All the samples were ground using SiC papers up to 1200 grit. The samples were subsequently cleaned ultrasonically with acetone and rinsed with distilled water to avoid surface contamination. The alloy samples were soaked in 100 ml of 5 M NaOH aqueous solution at 85 ^{o}C for 3, 6 and 12 h, and they were named respectively as KT3, KT6 and KT12 film, respectively. After removal from the solution, the samples were gently rinsed with ultrapure water for 30 s and dried at 40 ^{o}C.

2.2 Coating structure and phase composition analysis

Surface and cross-section morphologies of the films were analyzed using a scanning electron microscope (SEM, S-4800, Hitachi Co., Japan). The elemental composition of the films was also investigated with an energy dispersive spectrometer (EDS). Phase composition of the films was analyzed by X-ray diffraction (XRD) (Philips, X'Pert, The Netherlands) using Cu Kα radiation. The angle of the incident was fixed at 2°against the surface of the samples and the measurements were performed with a continuous scanning mode at a rate of 4°/min.

2.3 Bonding strength

The bonding strength between the films and the substrate were determined by a pull-off method ultilizing an Instron instrument. Parallel aligned cylinders were glued to the coated and back sides of the samples with epoxy resin. The pull-off force F needed to detach the film from the substrate with the contact area S was measured. Coating adhesion strength was estimated as F/S. The average bonding strength of each sample was obtained from five measurements.

2.4 Electrochemistry test

Table 1. Ion concentration of the SBF and human blood plasma

Ionic species	SBF (mmol/L)	Blood plasma (mmol/L)
Na^+	142.0	142.0
K^+	5.0	5.0
Mg^{2+}	1.5	1.5
Ca^{2+}	2.5	2.5
Cl^-	147.8	103.8
HCO_3^{2-}	4.2	27
HPO_4^{2-}	1.0	1.0
SO_4^{2-}	0.5	0.5

The corrosion resistance of the samples were evaluated by potentiodynamic polarization and electrochemical impedance spectroscopy (EIS) tests by a PARSTAT 2273 automatic laboratory corrosion measurement system, in which the samples with an exposed area of 10 mm ×10 mm was immersed in a simulated body fluids (SBF) solution. The SBF solution was prepared by dissolving analytical-grade chemicals of $NaCl$, KCl, Na_2SO_4, $NaHCO_3$, $K_2HPO_4 \cdot 3H_2O$, $MgCl_2 \cdot 6H_2O$, and $CaCl_2$ in distilled water and buffered at pH 7.4 with tris-hydroxymethyl aminomethan and 1 M HCl at 37 °C. The ion concentrations of the SBF used in the study are given in Table 1. Electrochemical tests were carried out using a three-electrode cell with a saturated calomel as a reference, a platinum plate as the counter and the specimen as the working electrode. Prior to the beginning of the test, the samples were kept in the solution for 0.5 h to make the open circuit potential stability. Potentiodynamic polarization

tests were performed, starting at −250 mV with reference to OCP at a sweep rate of 0.5 mVs^{-1} to a final current density of 0.1 mAcm^{-2}. Electrochemical impedance spectroscopy (EIS) studies were performed at open circuit potential with an AC amplitude of 10 mV over the frequency range of 10,000–0.01 Hz. The values of relevant components were fitted by using Zview software from Scribner Associates, Inc.

3. RESULTS

3.1 Morphology and composition of the coatings

Surface morphologies of the samples after alkaline treatment for 3, 6 and 12 h, respectively, are shown in Fig. 1. As shown in Fig. 1(a), the coating is dense and compact, traces of the scratches formed during the mechanical polishing before the alkali treatment are observed. At a higher magnification (inset in Fig. 1(a)) of the KT3 film, the different size pores are randomly distributed in the film, but the pores are very shallow. These pores on the film can be mainly divided into two types, one are large pores with about 1-2 μm diameter, and the others are small pores with nanometer scale. The large pores relate to the scratches before alkali treatment. And the small pores may be caused by the gas escaped from the coating. As seen in Fig. 1(b), no pores can be observed from both low and high magnifications. The as-deposited coating is dense, smooth, and uniform. At a low magnification, the surface of the KT12 film is dense and compact, but the film is rougher than KT6 film. At a higher magnification, there are some tiny erect flakes distributed on the surface, mainly due to crystallizations from amorphous.
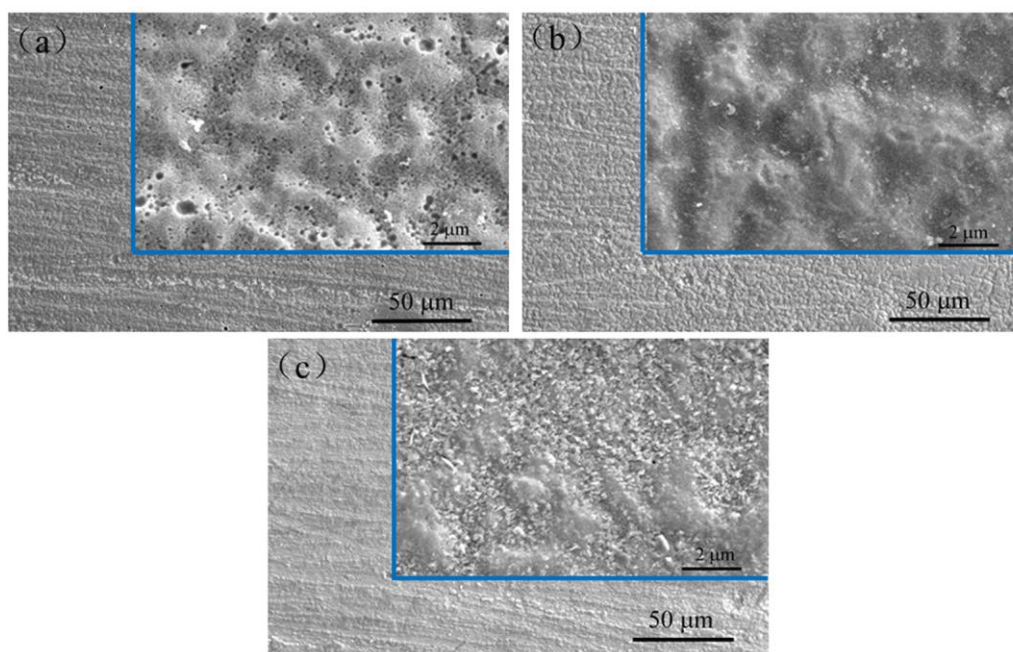

Figure 1. Surface morphologies of the films formed in different treatment time

The relative contents of elements in the coatings are shown in Table 2. The content of O, Mg and Al is described as a function of the treatment time. It is observed that the content of O increases with the treatment time, and the content of Mg, Al decrease with the treatment time.

Table 2. The element composition of the films

Element	Atomic concentration (%)		
	KT3	KT6	KF12
O	10.43	15.56	19.24
Mg	86.75	82.22	78.99
Al	2.82	2.22	1.78

The cross-section morphologies of the samples produced at different time are shown in Fig. 2(a)-(c), it can be found that the coatings bound firmly with the magnesium alloy substrate. There are no cracks or pores can be found in the in the figures. The sample treated for 3 h shows the formation of an 8 μm thin film (Fig. 2(a)). The thickest film (70 μm) is formed by treating for 12 h (Fig. 2(c)). The cross sections of the films indicate a regular increase in film thickness with increasing the treatment time.
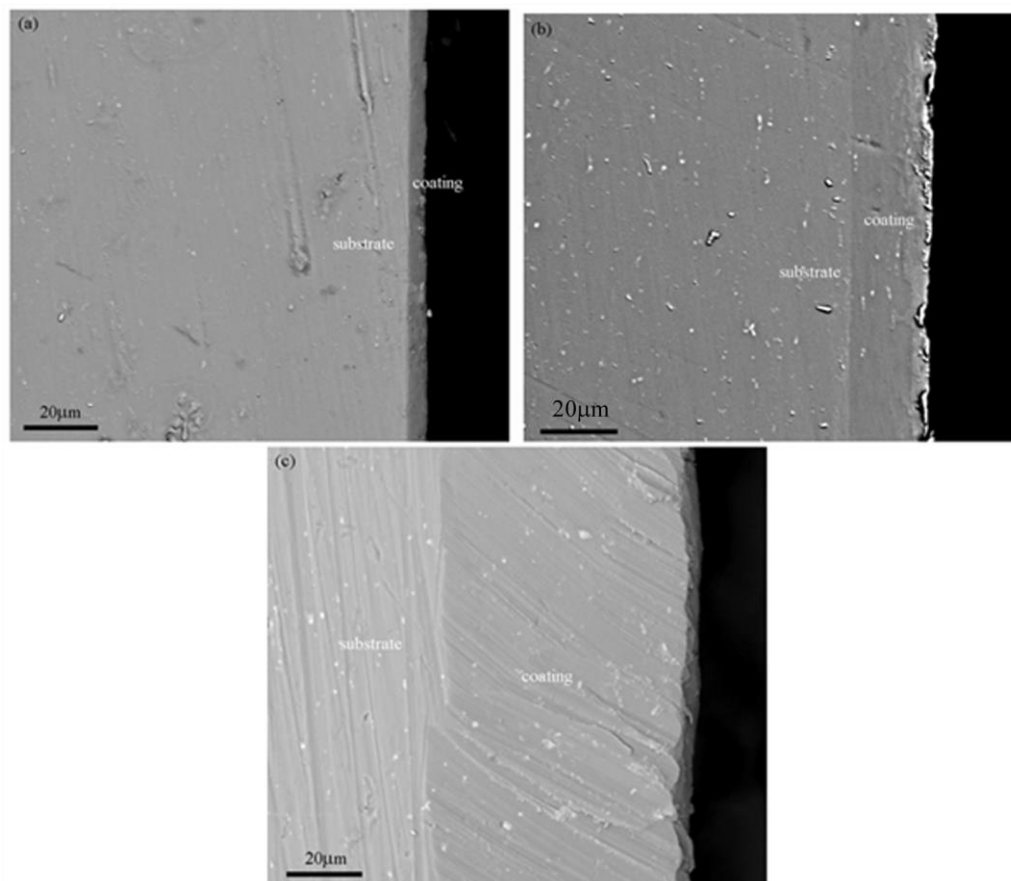

Figure 2. Cross-section morphologies of the films formed in different treatment time

3.2 Phase composition of the coatings

Fig. 3 shows the XRD patterns of the films formed by alkali treated for 3, 6 and 12 h, respectively. It is clearly shown that the films produced by alkali treatment are mainly composed of $Mg(OH)_2$. The relative content of $Mg(OH)_2$ in the film may be judged according to the intensity ratio of their strongest peaks (calculated by the peak height) in XRD patterns. It can be seen that the relative content of $Mg(OH)_2$ in the films increased with the time scale.
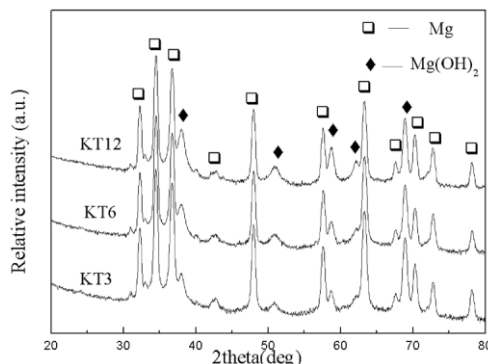

Figure 3. XRD patterns of the films under different treatment time

3.3 Bonding strength

Adhesion of the films with the magnesium substrate is one of the most essential properties for the implantation. The bonding strength of the alkali treatment films to the substrate magnesium alloys is shown in Fig. 4. It is clearly that the bonding strength of the films is decreased with increasing the treatment time. The bonding strength of the films decreases from 57.8 MPa for alkali treated 3 h, to 50.2 MPa for treated 6 h and 47.6 MPa for treated 12 h.
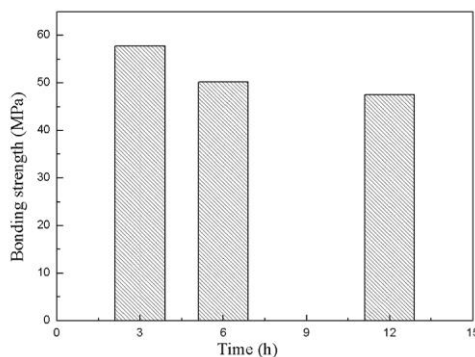

Figure 4. Bonding strength of the films prepared under different treatment time

Fig. 5 shows the typical detached surfaces after the adhesion test. A mixed failure mode is observed, which consists of epoxy failure and epoxy coating interface failure. The films are not

stripped from the substrate, and are completely intact. This indicates that the "true" bonding at the film-substrate interface should be stronger than that of the epoxy itself ($\geq$60 MPa).
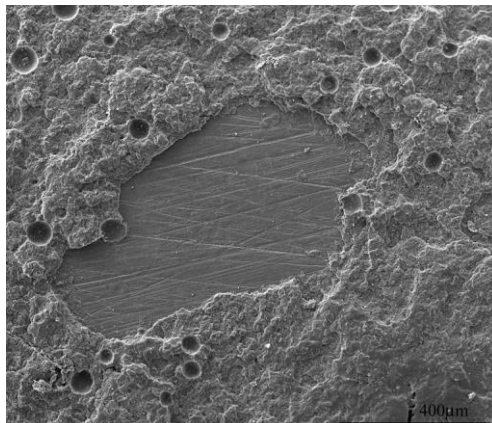

Figure 5. SEM photographs of the fractured surface after bond strength test

3.4 Electrochemical study

The typical electrochemical polarization curves of the AZ31 magnesium alloy and the alkali treatment films are obtained in SBF at 37°C, as plotted in Fig. 6. The date of the corrosion potential (E_{corr}), the corrosion current density (I_{corr}), and anodic/cathodic Tafel slopes (βa and βc) were extracted from Fig. 6 are shown in Table 3. In generally, the cathodic polarization curves is associated with the cathodic hydrogen evolution through water reduction, while the anodic polarization curves is attributed the dissolution of magnesium. It can be observed in Table3, anodic Tafel slope βa of alkali treatment samples is much bigger than that of blank substrate, which indicates that the alkali treatment films can restrain the anodic potential reaction. While their cathodic Tafel slopes βc are approximate, indicating that the cathodic hydrogen evolution has little different. Further, as seen in Table3, all the coated AZ31 magnesium alloys have a dramatic increase in corrosion resistance, which is evidenced by a shift of the whole polarization curves towards the region of lower current density and higher potential compared with the uncoated AZ31 magnesium alloy. The corrosion potential (E_{corr}) of the substrate with alkaline treated 3 h is shifted positively about 320 mV compared with substrate, and the corrosion current density (I_{corr}) decreased from 11.8 μm/cm^2 for the substrate to 3.17 μm/cm^2. With the treatment time, the corrosion potential (E_{corr}) of the films shift to more positively, lower corrosion current density, this is probably due to the enhancement in the film thickness, while maintaining its compactness. All of the (I_{corr}) values of the films is about one order lower than that of AZ31 magnesium alloy. It can be seen that the corrosion resistance of the Mg alloy significantly improved after alkali treatment. The enhancement of the corrosion resistance is related to the formation of Mg(OH)$_2$ barrier layer on the substrate, which can inhibit the corrosive ions penetrating into the substrate. Based on the Tafel studies, we can conclude that the alkali treatment technique is an effective method to enhance the corrosion resistance of magnesium alloy in SBF.
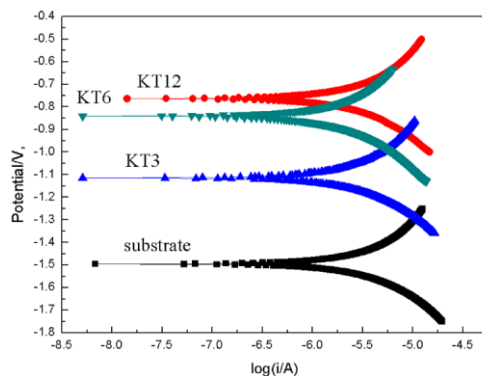
Figure 6. Potentiodynamic polarization tests of the samples in SBF solution

Table 3. The results of potentiodynamic polarization test in SBF solution

Samples	βa (mV/decade)	βc (mV/decade)	E_{corr} (V)	I_{corr} (A/cm^2)	R (Ω.cm^2)
sub	361	675	-1.48	1.18×10^{-5}	3566.4
KT3	497	509	-1.16	3.17×10^{-6}	11648.4
KT6	487	543	-0.87	2.02×10^{-6}	20840.2
KT12	491	501	-0.78	1.67×10^{-6}	26261.9

The EIS characteristics of the uncoated and coated samples in SBF solution are examined respectively at an open-circuit potential to illuminate the different corrosion resistance, as showed in Fig. 7. It can be clearly observed that the EIS diagrams are characterized by tow capacitive loops, which reflect two phenomenons with two different constant times. The first one at high frequency is assigned to the charge transfer reaction of the magnesium corrosion process. Another one appears at low frequencies and can attributed to the diffusion process across the corrosion layer or the anodic oxide on the surface.
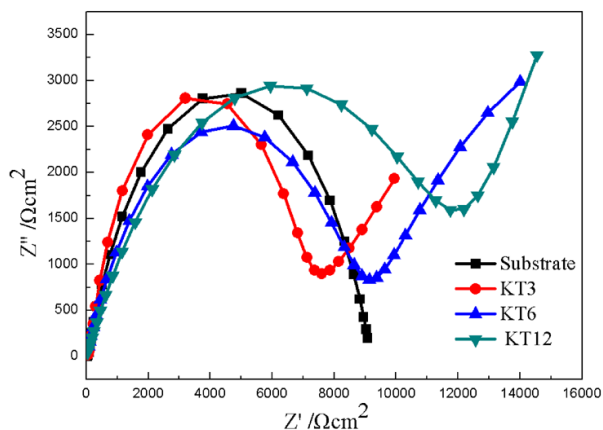

Figure 7. EIS spectra of bare magnesium alloy and the films

According to the special morphological structure of the coatings and the characteristic of the EIS diagrams, the EIS equivalent circuits for the coatings are proposed, as showed in Fig. 8. Rs represents the resistance of the electrolyte solution. R_1 and the constant phase elements (CPE Q_1) correspond to the resistance of the alkali treatment film. R_2 and the constant phase elements (CPE Q_2) associate to the charge transfer process at the metal/electrolyte interface. The (CPE Q) is a phase element related to the dispersion of a capacitance around a mean value. By fitting the equivalent circuit with the EIS spectra, a group of fitting parameters can be obtained to simulate EIS spectra of uncoated and coated samples achieved under different treatment time (Table 4). It can be seen from the table that the corrosion resistance of magnesium alloy is increased by 2-8 orders after alkali treatment due to the formation of alkali treatment films on magnesium alloy AZ31 substrate, and the corrosion resistance increases with increasing the treatment time.
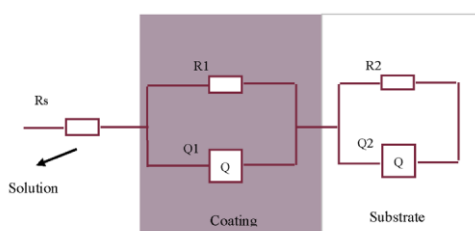

Figure 8. Simplified structure sketch of alkali treatment

Table 4. Fitting Results of EIS Plots of the Magnesium Alloy AZ31 and alkali treatment films

samples	R_s $(\Omega.cm^2)$	Q_{1-Y0} $(\Omega^{-1}.cm^{-2}.s^{-n})$	Q_{1-n}	R_1 $(\Omega.cm^2)$	Q_2-Y_0 $(\Omega^{-1}.cm^{-2}.s^{-n})$	Q_{2-n}	R_2 $(\Omega.cm^2)$
sub	411				1.9×10^{-5}	0.8	9.2×10^3
KT3	8.4	1.2×10^{-3}	0.8	8.2×10^3	9.8×10^{-6}	0.56	1.2×10^4
KT6	7.2	4.8×10^{-4}	0.5	2.6×10^4	1.4×10^{-6}	0.64	8.9×10^3
KT12	30.9	6.1×10^{-5}	0.3	6.4×10^4	3.6×10^{-6}	0.87	6.4×10^3

4. DISCUSSION

Magnesium is attractive implant material because it spontaneous degrades in physiological environment, and new bone growth replaces the Mg implant without producing any toxic byproducts. However, the degradation rate of Mg is generally faster than the bone generation rate, causing the losing of their mechanical property before the healing of bone tissue. In this study, magnesium hydroxide layers were formed on the surface of AZ31 magnesium substrate via alkali treatment in order to enhance the corrosion resistance. The formation of magnesium hydroxide layers on the surface of AZ31 magnesium alloy can be explained on the following process. In the heating alkali solution environment, Mg is oxidized ($Mg \rightarrow Mg^{2+} + 2e^-$), and the electrons produced by Mg oxidation are consumed by the reduction of water ($2H_2O + 2e^- \rightarrow 2OH^- + H_2$). And the hydroxide deposited on the

surface ($Mg^{2+} + 2OH^- \rightarrow Mg(OH)_2$). As these reaction take place on the whole surface of the alloy, a coating covering the entire surface is formed [22-24].

AZ31 magnesium alloy was immersed in alkali solution. Mg atoms and Al atoms were exposed, and galvanic cells were formed. Mg atoms converted into Mg^{2+}, the heat treatment accelerated this process. Some of these Mg^{2+} ions diffused into the solution, others remained their primary statins and reacted with OH- in the solution [25]. Initially, a small amount of $Mg(OH)_2$ grains were formed on the surface of the alloy. With the increase of the treatment time, a great number of $Mg(OH)_2$ grains were synthesized at the exposed surface and then aggregated. As a result, more and more $Mg(OH)_2$ grains were deposited on the surface, and the entire surface was covered by $Mg(OH)_2$ layer. During this process, the gas released according to the reaction, and many pores remained on the layer. Subsequently, OH^- ions permeated the initial layer by passing through the pores and reacted with the substrate. So the thickness of the layer increased with increasing the treatment time. The prior generated grains were modified by the solution via the process of dissolution and recrystallization as reported by Zhu et al. [26].

Published researches have obviously shown that the alkali treatment films are porous [27]. The pore formation was mainly due to the process of the gas escaping, in which the reaction between the OH^- and the Mg^{2+} acted as a driving force for gas escaping [28]. Generally, it is believed the surface and cross-section morphologies are influenced by the reaction temperature and treatment time. Higher temperature of alkali treatment can synthesize a thick $Mg(OH)_2$ layer in short time, which owing to the rapid reaction. And higher temperature treatment also leads to large size pore [29]. Increasing treatment time can form thicker film. It should be noted that some pores distributed on KT3 film. No pores can be observed on the surface of the KT6 film, and some tiny erect flakes distributed on the surface of KT12 film. This can be attributed by changing of the film formation rate along with the treatment time. In the first 3 hours, the film formation rate was very high, which accomplished mass of the gas escaping from the film. Subsequently, the formation rate of the film was slower than before because of the deposition of the film. To further increase in treatment time, film modified by the solution via the process of dissolution and recrystallization, so we can see some tiny erect flakes on the surface of KT12 film.

5. CONCLUSIONS

In the present investigation, compact and dense films are successfully grown on the substrate of AZ31 magnesium alloy by alkali treatment. The main component of the films is $Mg(OH)_2$. The thickness of the films increases with increasing the treatment time. The films bound firmly with the magnesium alloy substrate, and the bonding strength between the film and the substrate is stronger than 60 MPa. Compared with the bare magnesium alloy, alkali treatment coating has a higher potential, and a lower corrosion current density. It implies that the alkali treatment can signification improve the corrosion of AZ31 magnesium in SBF solution, the corrosion resistance of magnesium alloy increases with increasing treatment time. And Magnesium alloys with alkaline treated film may be expected to be a novel and promising as orthopedic implantation materials.

References

1. J. Hofstetter, E. Martinelli, A.M. Weinberg, M. Becker, B. Mingler, P.J. Uggowitzer, J.F. Löffler, *Corros. Sci*., 91 (2015) 29.
2. H. Hornberger, S. Virtanen, A.R. Boccaccini,, *Acta Biomater*. 8 (2012) 2442.
3. J.W. Lee, H.S. Han, K.J. Han, J. Park, H. Jeon, M.R. Ok, H.K. Seok, J.P. Ahn, K.E. Lee, D.H. Lee, S.J. Yang, S.Y. Cho, P.R. Cha, H. Kwon, T.H. Nam, J.H.L. Han, H.J. Rho, K.S. Lee, Y.C. Kim, D. Mantovani, *Pnas*., 113 (2016) 717.
4. R. Rojaee, M. Fathi, K. Raeissi, A. Sharifnabi, *Ceram. Int*., 40 (2014) 15149.
5. S. Virtanen, *Mater. Sci. Eng*., B. 176 (2011) 1600.
6. G.L. Song, *Corros. Sci*., 49 (2007) 1696-1701.
7. S.V. Dorozhkin, *Acta Biomater*., 10 (2014) 2919.
8. Chen YJ, Xu ZG, Smith C, Sankar *J. Acta Biomater*., 10 (2014) 4561.
9. Li B, Chen Y, Huang W, Yang WZ, Yin XS, Liu Y. *Ceram Int*., 42 (2016) 13074.
10. X. Zhang, X.W. Li, J.G. Li, X.D. Sun, *ACS Appl. Mater. Interfaces*., 6 (2014) 513.
11. J.L. Niu, G.Y. Yuan, Y. Liao, L. Mao, J. Zhang, Y.P. Wang, F. Huang, Y. Jiang, Y.H. He, W.J. Ding, *Mater. Sci. Eng*., C. 33 (2013) 4833.
12. M.B. Kannan, O. Wallipa, *Mater. Sci. Eng*., C. 33 (2013) 675.
13. K. Huang, S. Cai, G.H. Xu, M.G. Ren, X.X. Wang, R.Y. Zhang, S.X. Niu, H. Zhao, *Surf. Coat. Technol.*, 240 (2014) 137.
14. X.N. Gu, W. Zheng, Y. Cheng, Y.F. Zheng, *Acta Biomater*. 5 (2009) 2790.
15. V. Jokanovic´, M. Vilotijevic´, B. Jokanovic´, M. Jenko, I. Anzˇel, D. Stamenkovic´, V. Lazic, R. Rudolf, *Corros. Sci*., 82 (2014) 180.
16. E. Butev, Z. Esen, S. Bor, *Appl. Surf. Sci*., 327 (2015) 437.
17. Y.Y. Zhu, G.M. Wu, Y.H. Zhang, Q. Zhao, *Appl. Surf. Sci*., 257 (2011) 6129.
18. N. Kamiyama, G. Panomsuwan, E. Yamamoto, T. Sudare, N. Saito, T. Ishizaki, *Surf. Coat., Technol.* 286 (2016) 172.
19. J. Feng, Y. Chen, X.H. Liu, T.D. Liu, L.Y. Zou, Y.T. Wang, Y.M. Ren, Z.J. Fan, Y.Z. Lv, M.L. Zhang, *Mater. Chem. Phys*., 143 (2013) 322.
20. T. Ishizaki, N. Kamiyama, E. Yamamoto, S. Kumagai, T. Sudare, N. Saito, *J. Electrochem. Soc*., 162 (2015) 741.
21. R.K. Gupta, K. Mensah-Darkwa, D. Kumar, *J. Mater. Sci. Technol*., 30 (2014) 47.
22. G.L. Song, A. Atrens, *Adv. Eng. Mater*., 1 (1999) 11.
23. Q.F. Zong, L.D. Wang, W. Sun, G.C. Liu, *Corros. Sci.,* 89 (2014) 127.
24. Y.Y. Zhu, G.M. Wu, Y.H. Zhang, Q. Zhao, *Appl. Surf. Sci*., 257 (2011) 6129.
25. R.C. Zeng, L.J. Liu, K.J. Luo, L. Shen, F. Zhang, S.Q. Li, Y.H. Zou, *Trans. Nonferrous Met. Soc. China.*, 25 (2015) 4028.
26. Y.Y. Zhu, Q. Zhao, Y.H. Zhang, G.M. Wu, *Surf. Coat. Technol.*,206 (2012) 2961.
27. X.M. Zhang, G.S. Wu, X. Peng, L.M. Li, H.P. Feng, B. Gao, K.F. Huo, P.K. Chu, *Sci. Rep*. 5 (2015) 1.

28. Q. Zhao, W. Mahmood, Y.Y. Zhu, *Appl. Surf. Sci.*, 367 (2016) 249.
29. F.B. Gong, J. Shen, R.H. Gao, X. Xie, X. Luo, *Appl. Surf. Sci.*, 365 (2016) 268.